Cellular and Molecular Bioengineering, Vol. 12, No. 5, October 2019 *(© 2019)* pp. 357–373
https://doi.org/10.1007/s12195-019-00576-1

Dual Inhibitors-Loaded Nanotherapeutics that Target Kinase Signaling Pathways Synergize with Immune Checkpoint Inhibitor

ANUJAN RAMESH,[1] SIVA KUMAR NATARAJAN,[4] DIPIKA NANDI,[2] and ASHISH KULKARNI [1,2,3,4]

[1]Department of Chemical Engineering, University of Massachusetts, Amherst, MA, USA; [2]Department of Veterinary and Animal Science, University of Massachusetts, Amherst, MA, USA; [3]Center for Bioactive Delivery, Institute for Applied Life Sciences, University of Massachusetts, Amherst, MA, USA; and [4]Division of Engineering in Medicine, Department of Medicine, Brigham and Women's Hospital, Harvard Medical School, Boston, MA, USA

(Received 15 February 2019; accepted 15 May 2019; published online 21 May 2019)

Associate Editor Michael R. King oversaw the review of this article.

Abstract

Introduction—Immune checkpoint inhibitors that boost cytotoxic T cell-based immune responses have emerged as one of the most promising approaches in cancer treatment. However, it is increasingly being realized that T cell activation needs to be rationally combined with molecularly targeted therapeutics for a maximal anti-tumor outcome. Currently, two oncogenic drivers, MAPK and PI3K-mTOR have emerged as the two main molecular targets for combining with immunotherapy. However, there are major challenges in enabling such combinations: first, such combinations can result in high rates of toxicity. Second, while, these molecular targets could be driving tumor progression, they are essential for activation of the immune cells. So, the kinase inhibitors and immunotherapy can antagonize each other.

Objectives—We rationalized that the synergistic combination of kinase inhibitors and immunotherapy could be enabled by dual inhibitors-loaded supramolecular nanotherapeutics (DiLN) that can co-deliver PI3K- and MAPK-inhibitors to the cancer cells and activate immune response by T cell-modulating immunotherapy, resulting in greater anti-tumor efficacy while minimizing toxicity.

Methods—We engineered DiLNs by designing the amphiphilic building blocks (both drugs and co-lipids) that enables supramolecular nanoassembly. DiLNs were tested for their physiochemical properties including size, morphology, stability and drug release kinetics profiles. The efficacy of DiLNs was tested in drug-resistant cells such as $BRAF^{V600E}$ melanoma (D4M), Clear cell ovarian carcinoma (TOV21G) cells. The tumor inhibition efficiency of DiLNs in combination with immune checkpoint inhibitor antibody was studied in syngeneic D4M animal model.

Results—DiLNs were stable for over a month and released the drugs in a sustained manner. *In vitro* cytotoxicity studies in D4M and TOV21G cells showed that DiLNs were significantly more effective than free drugs. *In vivo* studies showed that the combination of DiLNs with anti PD-L1 antibody resulted in superior antitumor effect and survival.

Conclusion—This study shows that the rational combination of DiLNs that target multiple oncogenic signaling pathways with immune checkpoint inhibitors could emerge as an effective strategy to improve immunotherapeutic response against drug resistant tumors.

Keywords—Immunotherapy, Supramolecular nanoparticles, Cancer, Kinase signaling, Combination therapy.

ABBREVIATIONS

PI3K	Phosphoinositide 3-kinase
mTOR	Mammalian target of rapamycin
MAPK	Mitogen-activated protein kinase kinase

Address correspondence to Ashish Kulkarni, Department of Chemical Engineering, University of Massachusetts, Amherst, MA, USA. Electronic mail: akulkarni@engin.umass.edu

Ashish Kulkarni is an Assistant Professor in the Department of Chemical Engineering at the University of Massachusetts Amherst. Prior to this, he was an Instructor of Medicine at Harvard Medical School and Associate Bioengineer at Brigham & Women's Hospital. He obtained his B. Tech. in Chemical Technology from Institute of Chemical Technology, University of Mumbai and a PhD in Chemistry from University of Cincinnati, Ohio. He completed his postdoctoral training with Prof. Shiladitya Sengupta at Harvard Medical School and MIT. In Prof. Sengupta's laboratory, his research efforts were focused on the development of structure–activity relationship-inspired nanomedicine for cancer therapy. His lab is currently working on the development of tools and platform technologies for immunotherapy applications. His work has been published in *Nature Biomedical Engineering, Nature Communications, PNAS, ACS Nano* and *Cancer Research*, and featured in several science media outlets. He was recently selected as one of the top 12 rising researchers ('*Talented 12*') by American Chemical Society's (ACS) Chemical & Engineering News and '*NextGen Star*' in Cancer Research by American Association for Cancer Research (AACR). He is a recipient of several awards including American Cancer Society Research Scholar Award, Melanoma Research Alliance Young Investigator Award, Cancer Research Institute Technology Impact Award, Hearst Foundation Young Investigator Award, Harvard Cancer Center Career Development Award, AACR Scholar-in-training Award, American Society of Pharmacology and Experimental Therapeutics (ASPET) Young Scientist Award and Brigham & Women's Hospital Junior Faculty Mentor Award.

S.I. : 2019 Young Innovators Issue

Anujan Ramesh and Siva Kumar Natarajan contributed equally to this study.

1865-5025/19/1000-0357/0 © 2019 Biomedical Engineering Society

SNP	Supramolecular nanoparticles/nanotherapeutics
EGFR	Epidermal growth factor receptor
D4M	Dartmouth murine mutant malignant melanoma-3A
Akt	Protein kinase B
RTK	Receptor tyrosine kinase
PD-L1	Programed death ligand 1
MAPK	Mitogen-activated protein kinases
Erk	Extracellular signal-regulated kinase
mAb	Monoclonal antibody
FDA	Food and drug administration
PD-1	Programmed death protein 1
CTLA-4	Cytotoxic T-lymphocyte-associated protein 4
OCCC	Ovarian clear cell carcinoma
PBMCs	Peripheral blood monomorphonuclear cells
PBS	Phosphate buffered saline
TUNEL	Terminal deoxynucleotidyl transferase (TdT) dUTP nick-end labeling
NiR	Near infra-red
OCT	Optimal cutting temperature

INTRODUCTION

Cancer is one of the leading causes of death in the United States. Despite recent advances in cancer therapies, the number of cancer related deaths in the United States is still alarmingly high, with nearly 609,640 deaths reported in 2018.[43] Conventional cancer therapeutics are often associated with high systemic toxicities even at low therapeutic doses leading to poor quality of life.[6] In addition to this, the inherent ability of cancers to develop drug resistance against conventional chemotherapeutics necessitates the need for alternative treatment methods.[17] Targeting the PI3-K—Akt or the MAPK signaling pathways seems to have emerged as an attractive approach for cancer drug development in recent times.[36] The PI3K oncogene is dysregulated in a large number of cancers.[12] This ubiquitously activated signaling pathway has an array of functions in cancer, including involvement in growth, proliferation, cancer stem cell differentiation and angiogenesis.[19] Interestingly, the Ras-MAPK signaling cascade is another RTK mediated signaling pathway responsible for cellular mechanisms involved in proliferation and growth.[9] MAPK is also highly dysregulated in cancer cells and is usually activated by the binding of cytokines and growth factor to EGFRs on the cytoplasmic surface.[39] The role of MAPK and PI3K is of particular importance in cancers like melanoma and ovarian clear cell carcinoma.[18,25,28] Kinase mutations in melanomas are highly prevalent with over 75% of melanoma cells expressing mutations in BRAF and RAS genes.[14] In addition to this, malignant melanoma is a highly aggressive cancer, with high incidence rates followed by high mortality. Ovarian clear cell carcinomas also have high incidences of KRAS (27–36%) and BRAF mutations (33–50%).[3] Recent studies have shown that mutations in downstream kinases of the EGFR pathway like B-Raf and K-Ras have been linked with increased chemotherapeutic resistance.[10,15] Ras mutations which activate downstream Erk kinases leads to increased proliferative activity of the cells, whereas activation of Akt is involved in an anti-apoptotic signaling which enhances cell survival (Suppl. Fig. 1).[45] The cross-dependent nature of these pathways translates to increased survival and proliferation in the presence of chemotherapeutic drugs.

Targeted therapies involving kinase inhibitors like PI3K and MAPK inhibitors, are usually characterized by high response rates.[8,31,55] The discovery of these kinase mutations in aggressive cancer models led our hypothesis that kinase inhibitors for anti-cancer therapy might prove to be an effective strategy. However clinical trials involving PI3K inhibitors as a monotherapy showed underwhelming results. Monotherapeutic PI3K inhibiting drugs like SAR24548(XL147), PX-866 and GDC-0941 used in clinical trials for treatment of solid tumors, showed modest responses on tumor apoptosis, with no real no correlation between inhibition of PI3K and the outcome.[16,40,41] MAPK inhibitors like C1-1040, PD0325901 and AZD6244 also demonstrated poor efficacy in pre-clinical and clinical trials.[18] This poor efficacy could be attributed to systemic toxicities, low bioavailability and hepatic metabolism.[18] Previously, both these pathways were considered to be linearly independent pathways. However, it has since been established that both these pathways communicated with each other and engaged in cross talk.[32] These pathways were able to compensate each other through a positive and negative feedback loops. Furthermore, patients administered with these drugs relapsed post-treatment and the drugs did not exhibit sustained anti-cancer efficacy. Thus, we rationalized that simultaneous inhibition of both the pathways could significantly improve the response.[32]

Aggressive cancers like melanoma are generally characterized by poor prognosis and develop resistance against targeted therapies, thereby hinder the therapeutic efficacy.[30] Immunotherapy on the other hand showed limited, but long-term survival benefits against aggressive cancers like melanoma.[21] Monoclonal antibody therapies (mAbs) targeting Immune checkpoint blockade has emerged as a powerful treatment options

after long lasting responses were observed in clinical trials which led to recent FDA approvals.[21] CTLA-4 blockade using mAbs was the first immune checkpoint therapy to get FDA approval.[21] The PD1 – PDL1 axis was also identified to be a potential target in immune checkpoint blockade. Nivolumab, a PD-L1 immune checkpoint blocker and ipilimumab, a CTLA-4 blocker was successfully used to treat patients with melanoma.[37,46] These therapies showed long term and durable anti-cancer efficacy followed by curative tumor regression. These effects also persisted long after the drug discontinuation.

Even with early promising results, immunotherapy is still limited as a monotherapy due to its lower response rates.[2] Ipilimumab had a dismal response rate of only 17% and Nivolumab had a response rate of 31%.[37,46] These limitations demand for the need for a rational combination therapy strategies, which can effectively combine the high response rates of targeted treatments with long term durability of immunotherapy. One of the major challenges in enabling this combination is the fact that both the MAPK and the PI3K pathways play an important role in T cell function and proliferation.[20,42] MAPK plays a crucial role in T cell differentiation and lineage commitment along with T cell receptor recognition and activation.[42] Moreover, studies have shown that the PI3K pathway plays a central role in CD8+ T cell clonal expansion into effector and memory CD8+ T cells.[20] Thus, a systemic inhibition of these pathways using free kinase inhibitors could affect the viability and activation of systemic naïve T cells, potentially limiting the use of T cell activating immunotherapy including immune checkpoint inhibitor antibodies.

To offset these limitations, nanoparticle systems for delivery of kinase inhibitors offer an exciting alternative. Nanoparticles can be designed to have optimal size and surface properties which can help increase its lifespan in systemic circulation.[7] It can also be used to carry inhibitors which have low water solubilities and low therapeutic indices.[23] Nanoparticles preferentially accumulate into the tumor microenvironment using the leaky vasculature associated with pathophysiology of the tumor in what is termed as enhanced permeability and retention (EPR) effect.[7] This enhances the bioavailability of the active drug component while at the same time minimizes systemic toxicity. Additionally, we anticipated that the nanoparticles could induce sustained inhibition of PI3K and MAPK signaling in cancer cells.[4] Here, we report a dual inhibitors-loaded supramolecular nanotherapeutic (DiLNs), loaded with kinase-inhibiting amphiphiles (PI3K and MAPK) and demonstrate its efficacy in drug resistant aggressive cancers like ovarian clear cell carcinoma (OCCC) and $BRAFV^{600E}$ melanoma. We have also studied the synergistic effect of combining immune checkpoint blockades with DiLNs. We demonstrated that the DiLNs are more effective than free inhibitors combination and individual inhibitor loaded nanotherapeutics in both OCCC and melanoma. Interestingly, the DiLNs showed minimum cytotoxicity to T cells as compared to the free drugs and had no effect on the activity of T cells. We further demonstrated that DiLNs synergistically combine with immune checkpoint inhibitor antibody to enhance anti- tumor efficacy in aggressive $BRAFV^{600E}$ melanoma model.

MATERIALS AND METHODS

Reagents and Instruments

All materials were pure and analytical grade. Dichloromethane (DCM), methanol, and *N*, *N*-dimethylformamide (DMF) were purchased from Fisher Scientific. 4-dimethylaminopyridine (DMAP), L-α-phosphatidylcholine (PC), and Sephadex G-25 were purchased from Sigma-Aldrich.1,2-Distearoyl-sn-Glycero-3-Phosphoethanolamine-*N*-[Amino(Polyethylene Glycol)2000](DSPE-PEG-Amine), cholesterol hemisuccinate and mini hand-held extruder kit was bought from Avanti Polar Lipids. 0.4 and 0.2 μm Nucleopore Track-Etch Membrane and 10 mm Filter supports and 250 ml Syringes were bought from Avanti Polar Lipids. 1-Ethyl-3-(3-dimethylaminopropyl) carbodiimide (EDC) was purchased from Acros Chemicals. PI-103 and Selumetinib was purchased from LC Laboratories. Anti-PDL1 antibody was purchased from Biolegend Inc. Analytical thin-layer chromatography (TLC) was performed using precoated silica gel aluminum sheets 60 F254, purchased from Sigma-Aldrich. Spots on the TLC plates were visualized under UV light. MTS Reagent and Phenazine metho-sulfate was bought from Promega. 6 wells and 12 wells, 5 mL, and 10 mL plates were purchased from Corning. DMEM, FBS, and antibiotic–antimycotic were purchased from Gibco, Life Technologies. Phospho Erk1/2, total Erk1/2, phospho AKT, total AKT, and beta actin antibodies were purchased from Cell Signaling Technology. CD8a, CD4, CD62L, CD44 antibodies were bought form Biolegend Inc. Mouse anti Rat CD8a Primary and Alexa Flour 488 Goat Anti Rat Secondary antibody was purchased from Thermo Fisher. UV–Vis absorption spectra were obtained using Shimadzu UV3600 UV–Vis Spectrophotometer. Electron microscopy was performed using a FEI Tecnai Cryo-Bio 200 kV FEG TEM and confocal microscope images were taken with Nikon A1SP Spectra. Hydrodynamic size and zeta potential were measured using Malvern Zetasizer Nano ZSP.

MTS assay was performed using a BioTek plate reader. Flow cytometric analysis was performed using ACEA Novocyte Flow cytometer and the data was analyzed using the NovoExpress software.

Synthesis of PI3K and MAPK Inhibiting Amphiphile

PI103 or Selumetinib was dissolved in 2 mL anhydrous DCM along with 1.1 molar equivalents of cholesterol hemisuccinate, DMAP, and EDC. The reaction was stirred at room temperature under inert conditions for 24 h. The progress of the reaction was monitored through thin-layer chromatography (TLC) at different time intervals over 24 h. Once the reaction was completed, the corresponding final product was purified through column chromatography by eluting with a 3% methanol: 97%DCM gradient, to get the PI3K or MAPK -inhibiting amphiphile as pale-yellow color. The final products were analyzed by ^{1}H NMR and Mass spectrometry for purity and structural integrity and confirmed with previously reported values.

Synthesis and Characterization of DiLNs

DiLNs were synthesized using lipid-film hydration method. Briefly, L-α-phosphatidylcholine (PC), DSPE-PEG-Amine, and kinase inhibiting amphiphiles at 6:3:1 molar ratio was dissolved in 1 mL DCM. For single-inhibitor loaded supramolecular nanoparticles, 10 mol% of either PI3K-inhibiting amphiphile or MAPK-inhibiting amphiphile was used. DiLNs were comprised of 5 mol% of each PI3K and MAPK inhibiting amphiphiles. The solvent was evaporated to form a thin film followed by hydration with PBS at 60 °C for 2 h to obtain self-assembled supramolecular nanotherapeutics loaded with either single or dual kinase inhibitors. The supramolecular nanotherapeutics were then extruded through a 0.4 and 0.2 μm polycarbonate membranes using a mini-extruder. The hydrodynamic diameter was measured by Dynamic Light Scattering and the drug loading efficiency of the nanoparticles was measured by UV–Vis Spectrophotometer.

DiLNs Stability Studies

DiLNs were incubated with equal volumes of human serum or PBS at 4 °C. The stability of DiLNs in either serum or PBS was calculated by measuring the average hydrodynamic diameter and zeta potential of the SNPs using Malvern Zetasizer Instrument at specified time intervals.

Drug Release Kinetics Studies

P13K inhibiting amphiphiles or MAPK inhibiting amphiphiles (1 mg inhibitor combination/mL, 5 mL) were suspended in PBS buffer (pH 7.4) or acidic buffer s (pH 5.4) or TOV21G cell lysate (pH 5–6) and sealed in dialysis tube (MWCO = 3500 Da, Float-A-Lyzer, Spectrum Labs). Sealed dialysis tubing was suspended in 500 mL of PBS with gentle stirring to simulate the infinite sink tank condition. 100 μL portions of the aliquot was collected from the incubation medium at predetermined time intervals and replaced by equal amounts of PBS buffer. The portions taken from the dialysis tubing were analyzed using UV–VIS spectrophotometry and was plotted in terms of cumulative inhibitor release over several days.

Cryo-Transmission Electron Microscopy for DiLNs

DiLNs samples were preserved using a Vitrobot and liquid ethane. Briefly, the sample was prepared on plasma treated lacey carbon 400-mesh copper grids. 5 μL of nanoparticle suspension was placed onto the plasma treated grids, subsequently blotted with filter paper and processed by vitrification in liquid ethane. Electron microscopy was performed using a Phillips CM 120 Cryo operating at 120 keV using a Gatan Oris 2 k by 2 k CCD camera system. Vitreous ice grids were transferred into the cryo-electron on a cryostage that maintains the grids at a temperature below − 180°C. Images were acquired at 66 kx (0.152 nm pixels) under low-dose conditions at 8–10 electrons Å^{2}.

Cytotoxic Efficacy of DiLNs Using MTS Assay

10×10^{3} TOV21G cells or D4M cells per well were seeded in a 96 well plate, and left overnight to adhere. The cells were serum starved for 6 h by incubating them in serum free basal medium. The cells were incubated with either free drugs or DiLNs of equivalent free drug concentrations for 72 h. The cells were washed with PBS and the medium was replaced with phenol red free DMEM followed by incubation in a mixture of MTS and PMS (1:20) solution for 30 min. Absorbance was measured at 480 nm using a BioTek plate reader. The data was analyzed using graph pad.

Cytotoxic Efficacy of Blank DiLNs Using MTS Assay

10×10^{3} D4M cells per well were seeded in a 96 well plate, and left overnight to adhere. The cells were serum starved for 6 h by incubating them in serum free

basal medium. The cells were incubated with blank DiLNs for 72 h. The cells were washed with PBS and the medium was replaced with phenol red free DMEM followed by incubation in a mixture of MTS and PMS (1:20) solution for 30 min. Absorbance was measured at 480 nm using a BioTek plate reader. The data was analyzed using graph pad.

Evaluation of DiLNs Internalization in D4M Cells

FITC-dye tagged DiLNs were synthesized. Briefly, 9 mol% of both the PI3K and MAPK-inhibiting amphiphiles (4.5 mol% each), 1 mol% FITC-cholesterol conjugate, 30 mol% DSPE-PEG-Amine and 60 mol% PC were dissolved in 1 mL of DCM, followed by formation of the thin film by evaporation of DCM. The lipid film was hydrated to form the supramolecular nanoparticles. The amount of FITC-cholesterol present was determined using a fluorescence spectrometer. D4M cells were seeded at a density of 50×10^3 cells per well onto an 8-well chamber slide. The FITC tagged DiLNs were then added at 10 μM (dye concentration) and incubated for varying time points. After incubation, the cells were washed with PBS to remove the particles that were not internalized. Cells were fixed using 4% PFA and stained with DAPI followed by mounting using Invitrogen Glass Antifade reagent. Images were taken at 60x using a Nikon A1R-SIMe confocal microscope and were analyzed using NIS Elements 4.6.

Western Blot to Study Dual Kinase Inhibition Using DiLNs

2×10^5 cells were seeded in each well of a 6-well plate and incubated with free drug or DiLNs of equivalent free drug concentrations for varying periods of time. After incubation for the desired time period, the cells were lysed, and protein lysates were electrophoresed on a 10% polyacrylamide gel and transferred to a PVDF membrane followed by incubation with antibodies against phosphorylated forms of proteins (Phospho-p44/42 MAPK (Erk1/2) (1:1000 dilution), p44/42 MAPK (Erk1/2) (1:2000 dilution), phospho-Akt (1:1000 dilution), Total-Akt (1:2000 dilution) and β-actin (1:1000 dilution) antibodies) overnight at 4 °C. After washing with TBST, membranes were incubated with horseradish peroxidase-conjugated secondary antibody (1:2000) for 1 h. Detection was done using Biorad's Clarity ECL and image processing was done by Image Lab and probed with horseradish peroxidase-conjugated secondary antibody.

Flow Cytometry Assay to Quantify Toxicity of DiLNs on T Cells

1.5×10^5 Human T cells were seeded per well in 12-well cells and were allowed to reach sub confluency. The cells were then treated with either free drug combinations or DiLNs (normalized to equivalent free drug combinations). Following the treatment, the cells were collected in media then washed and centrifuged in Annexin V buffer. The cells were incubated with Annexin V antibody and Propidium iodide as per manufacturer's protocol. Post staining, the cells were washed and analyzed using a Novocyte flow cytometer and the results were processed using NovoExpress v1.2.5. The cells were gated for a live population and isolated singlets in order to reduce autofluorescence from doublets. The singlets were then isolated out into separate populations to quantify the amounts of Annexin V negative cells to signify viability.

Flow Cytometry Assay to Quantify Toxicity of DiLNs on T Mouse Cells

1.5×10^5 mouse T cells were seeded per well in 12-well cells and were allowed to reach sub confluency. The cells were then treated with either free drug combinations or DiLNs (normalized to equivalent free drug combinations). Following the treatment, the cells were collected in media then washed and centrifuged in Annexin V buffer. The cells were incubated with Annexin V antibody and Propidium iodide as per manufacturer's protocol. Post staining, the cells were washed and analyzed using a Novocyte flow cytometer and the results were processed using NovoExpress v1.2.5. The cells were gated for a live population and isolated singlets in order to reduce autofluorescence from doublets. The singlets were then isolated out into separate populations to quantify the amounts of Annexin V negative cells to signify viability.

Effect of DiLNs on T Cells Activation

T cells were isolated from Human PBMCs using Human T cell enrichment kit according to manufacturer's protocol (StemCell Technologies). The cells were seeded on a 12-well plate in recommended medium (IL-2 supplemented RPMI 1640 medium) at the density of 100,000 cells/well and were treated with different concentrations of DiLNs or their combination free drugs. The cells were allowed to incubate for 36 h along with CD3/CD28 Dynabeads (for activation) according to the manufacturer's protocol (Thermo Fisher Scientific). The cells were then centrifuged at

2000 rpm and washed with PBS. After desired incubation period, the cell surface expressions of CD4 vs CD8 and CD44 vs CD62L were evaluated by surface staining and analyzed by an ACEA Novocyte Flow cytometer and results were processed using NovoExpress v1.2.5.

In Vivo Biodistribution Studies

DiR dye-labeled DiLNs were synthesized by lipid-film hydration method. Briefly, 60 mol% of PC, 9 mol% of the PI3K and MAPK-inhibiting amphiphiles, 1 mol % of DiR dye, and 30 mol% of DSPE-PEG-Amine were dissolved in 1.0 mL DCM. Solvent was evaporated into a thin and uniform lipid-drug film using a rotary evaporator. The lipid drugs film was then hydrated with 1.0 mL H_2O for 2 h at 60 °C. D4M (1×10^6 cells/mouse) were inoculated subcutaneously into the flank of each male C57B/L6 mice (4–6 weeks old, weight ~ 20 g). After the tumor reached ~ 500 mm^3 volume, dye-labeled DiLNs were injected through the tail vein of the tumor bearing mice. The imaging was performed at 1, 6, 24, and 48 h post-injection using IVIS filter set (excitation 710 nm and emission 760 nm). After the imaging, mice were sacrificed, and major organs were collected and imaged. All the images were captured using Maestro (CRI) small animal *in vivo* fluorescence imaging system. For the purposes of this study, the exposure times for acquiring the data were kept the same. Post experiment, the images were analyzed using the Maestro software, spectral unmixing was done to subtract the background autofluorescence of mouse tissues using an untreated mouse as a control. Relative fluorescence was quantified for each organ and plotted as a graph using Graph Pad.

In Vivo Efficacy Studies in D4M Mouse Model

D4M cells (1×10^6 cells per mouse) were injected subcutaneously into the right flank of C57B/L6 mice. The tumors were allowed to reach a size of ~ 75 mm^3 (10 days post inoculation) and the mice were randomized into different groups. The 1st treatment dose was started and will be now referred to as day 0. Vehicle, combination free drugs (PI103 + Selumetinib), Combination free Drugs + anti PDL1, DiLNs, DiLNs + anti PD-L1 [Normalized to the equivalent free drug concentrations] and free anti PDL1 antibody were administered at a dosage of 5 mg/kg of the drugs and 5 mg/kg of the antibody. The different doses were administered on days 0, 3, and 5. The tumor volumes were monitored throughout the entire treatment, every other day. In order to calculate the tumor volume, the volume of an ellipsoid was used ($L \times B^2/2$, L being the longest diameter of the tumor, B being the shortest) and measured using a Vernier caliper. Mice were sacrificed when tumor volumes reached either 2000 mm^3 or tumors exhibited necrosis or mice became lethargic. All animal procedures were approved by the BWH Institutional Animal Care and Use Committee (IACUC).

Western Blot of Tumor Samples from Different Treatment Groups

The excised tumors from different treatment groups were taken from the mice and flash frozen at − 80 °C. Samples were then resected, homogenized and lysed in ice-cold NP40 cell lysis buffer containing protease and phosphatase inhibitors. Centrifugation at 15,000 rpm was done in order to remove cellular debris and the supernatant was used for the rest of the experiment. BCA protein assay kit was used for protein estimation. 45 μg of protein was loaded in each well and were electrophoresed on a 10% polyacrylamide gel and transferred to a PVDF membrane, which were incubated with antibodies against phosphorylated forms of proteins (PPhospho-p44/42 MAPK (Erk1/2) (1:1000 dilution), p44/42 MAPK (Erk1/2) (1:2000 dilution), phospho-Akt (1:1000 dilution), Total-Akt (1:2000 dilution) and β-actin (1:1000 dilution) antibodies) overnight at 4 °C. After washing with TBST, membranes were incubated with horseradish peroxidase-conjugated secondary antibody (1:2000) for 1 h. Detection was done using Biorad's Clarity ECL and image processing was done by Image J and probed with horseradish peroxidase-conjugated secondary antibody. Expression was normalized to total expression of the specific protein or β-actin.

TUNEL Assay to Confirm In Vivo Cytotoxicity

Tumors from different treatment groups were excised, flash frozen and embedded into OCT blocks (Tissue Tek). 5 Micron sections were cut using a cryostat, and the sections were then fixed with 4% Paraformaldehyde and followed by staining with Alexa Fluor 588 Click -iT^{TM} Plus TUNEL Assay Kit (Thermo Fisher) as per the manufacturer's recommended protocol. Nuclei were stained with DAPI (Blue). Imaging was performed with Nikon A1R-SIMe confocal microscope at ×20 and analyzed with NIS Elements.

Imaging of Infiltrating CD8+ T Cells in Tumors

Tumors excised from treatment groups were flash frozen and embedded into OCT blocks. 5 Micron section were cut using a cryostat and these sections

were first fixed with ice-cold methanol for 10 min. After fixation, the sections were blocked using a solution of 1% BSA in PBST for 60 min. The sections were then probed for CD8a infiltrating T cells by incubating them with Rat anti mouse CD8a primary antibody (Thermo fisher) overnight at 4 °C. After the incubation period, the sections were washed and incubated with Alexa Four 488 goat anti rat secondary antibody (Thermo Fisher) for 2 h at Room temperature. The sections were washed and counter stained with DAPI and mounted using prolong glass antifade. Imaging was performed with Nikon A1R-SIMe confocal microscope at ×20 and analyzed using NIS Elements.

RESULTS AND DISCUSSION

Small molecular inhibitors of the PI3K and MAPK signaling pathways were widely studied and have been used in both clinical and pre-clinical trials as monotherapies.[1,33,38] However, such treatments showed limited response due to lack of sufficient and sustained inhibition of these pathways in cancer cells. Effective dose concentrations are limited by high incidence of systemic toxicity and drug resistance due to feedback signaling associated with MAPK/AKT pathways. Recent studies have shown that chemo-resistance activated through the PI3K pathway leads to increased PD-L1 expression which translates to efficient immune escape.[51,53] Combination therapies involving immune checkpoint inhibitors and targeted therapies provide an alternative option to monotherapies. However, high systemic T cell toxicities exhibited by small molecule inhibitors involved in targeted therapy may lead to ineffective immunotherapeutic efficacy. We rationalized that tumor specific delivery of combination of these inhibitors using DiLNs could lead to parallel and sustained inhibition of both the MAPK and PI3K pathways and could be combined with anti PD-L1 immune checkpoint inhibitor antibody. We anticipated that this could in turn lead to better anti-cancer efficacy (Fig. 1). We tested the *in vitro* efficacy of these drugs on highly aggressive and drug resistant cancer cells such as ovarian clear carcinoma cells (TOV21G cell line) and $BRAFV^{600E}$ D4M melanoma cells. We further tested the *in vivo* efficacy of DiLNs in combination with anti-PD-L1 antibody in a syngeneic and immunocompetent D4M Melanoma mouse model.

Synergistic Effect of Co-Inhibition of PI3K and MAPK Pathways in Drug-Resistance Cancer Cells

OCCCs are notoriously chemo-resistant and biopsies in ovarian carcinoma tumor samples reveal that these tumors in addition to existing RAF/RAS mutations, also overexpress Bcl-2 and p53, two proteins involved in the control of apoptosis leading to poor cancer prognosis.[11] Targeted therapies through kinase inhibition have proved to be effective against drug resistant cell lines.[44] However previous studies with $BRAFV^{600E}$ mutated cell lines show that inhibition of kinase signaling pathways using BRAF inhibitors were not effective.[50] Resistance to BRAF inhibition was observed through reactivation of MAPK pathways in Phase I clinical trials on BRAF mutated melanoma models.[27] Hence we rationalized that the use of an MAPK inhibitor, Selumetinib in combination with an PI3K inhibitor, PI103 would effectively inhibit both kinase pathways (Suppl. Fig. 2). In addition to melanoma, ovarian cancer cells also have BRAF mutations which makes them aggressive drug resistant cells through alternate activation of MAPK and PI3K pathway.[5,26] The PI3K signaling cascade is initiated due to the activation of receptor tyrosine kinases (RKTs). Activation of RKTs leads to downstream activation of class I_A PI3K isoforms which in turn initiates the downstream signaling cascade responsible for its oncogenic functions. Interestingly, the Ras-MAPK signaling cascade is another RTK mediated signaling pathway responsible for cellular mechanisms involved in proliferation and growth. RAS upon activation, acts as a messenger and relays extracellular signals to the nucleus through a set of phosphorylated events. RAS activation leads to downstream activation of Erk1/2 which further releases transcription factors associated with cellular proliferation.[12,48] We first wanted to test our hypothesis of dual kinase inhibition on ovarian clear cell carcinoma cell line (TOV21G). As shown in the western blot in Figs. 2a–2c, we observed a significant inhibition in expressions of phospho-Akt and phospho-Erk1/2 when treated with PI103 and Selumetinib respectively, which shows that the kinase signaling pathways are effectively inhibited. Next, we wanted to test if the inhibition of the signaling pathways correlated to effective cancer cell cytotoxicity. We treated TOV21G cells with either PI103, Selumetinib or an equimolar combination of both PI103 and Selumetinib and analyze cell toxicity after 72 h of incubation. As shown in Fig. 2d, we observed that dual kinase inhibitors were more effective as compared to their single drug counterparts. This further reinforces our hypothesis that parallel inhibition of both PI3K and MAPK simultaneously results in increased cytotoxicity of ovarian clear cell carcinoma cells. In addition to testing out the cytotoxic efficacy of equimolar concentration of both the drugs, we also wanted to study the cytotoxic effect of varying ratios of PI103: Selumetinib. We first studied the cytotoxic effects of varying concentration of Selumetinib keeping the concentration of PI103 constant and then studied

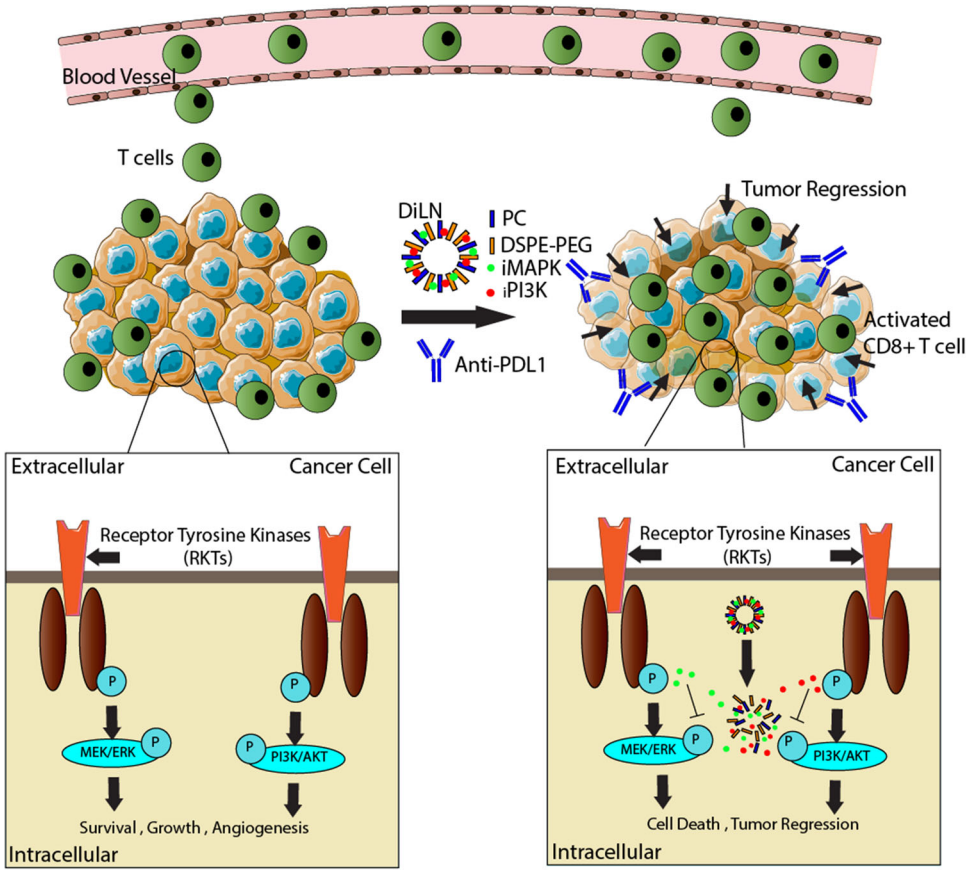

FIGURE 1. Schematic illustration of combination of Dual inhibitor-loaded Supramolecular Nanotherapeutics (DiLNs) with immune checkpoint inhibitor: Dual inhibitor-loaded supramolecular nanoparticles (DiLNs) accumulate into tumor microenvironment and deliver dual kinase-inhibiting molecules into the cancer cells. Sustained inhibition of PI3K and MAPK/Erk signaling pathways lead to efficient cytotoxicity in cancer cells. This in combination with an immune checkpoint inhibitor (anti-PDL1 antibody) activates the anti-tumor immune response, increases infiltrating cytotoxic T cells resulting and improves anti-tumor efficacy.

the effect of varying the concentration of PI103 and keeping the concentration of Selumetinib constant. As shown in the graphs in Figs. 2e and 2f, we demonstrated that a 1:1 combination of both Selumetinib and PI103 resulted in the most efficient and synergistic cytotoxic effect. Therefore, all further experiments involving combination of both the drugs were carried out using a 1:1 ratio of PI103: Selumetinib.

Synthesis and Characterization of DiLNs

In order to effectively inhibit both the MAPK and PI3K pathways concurrently and reduce toxicity associated with combination therapy, we wanted to co-deliver both the MAPK and PI3K-inhibiting drugs to the tumor. Previous studies have shown that free kinase inhibitors are plagued by limitations such as having low therapeutic indices and nonspecific biodistribution leading to non-targeted toxicity.[22,24] Furthermore, free drugs such as PI103 and Selumetinib are water insoluble and hence they need to be administered either orally or intra-peritoneally which leads to low bioavailability of the drugs at the site of the tumor. To offset these challenges, we hypothesized that a lipid-based supramolecular nanotherapeutic delivery system carrying both kinase inhibitors could result in improved anti-cancer efficacy. First, we checked if both the kinase inhibitors can be loaded in a traditional liposomal delivery system. 5 mol% of each of PI103 and Selumetinib was taken and the ratio of the drugs were kept at 1:1 as previously described. Liposomes with 60 mol% of PC and 30 mol% of DSPE-PEG-Amine along with the free drugs was made and it was observed that these liposomes were very unstable, and the drugs precipitated out within a few minutes (Fig. 3a). We concluded that the amount of free drugs loaded between the lipid bi-layers in a stable manner in this liposomal system was limited. Our earlier studies indicated that free inhibitors of drug concentrations above 5 mol% could not be effectively loaded into the liposomes.[22,24] These limitations however could be overcome by designing kinase inhibiting amphiphiles. In reference to our previous studies, we first designed kinase-inhibiting amphiphiles using an algorithm

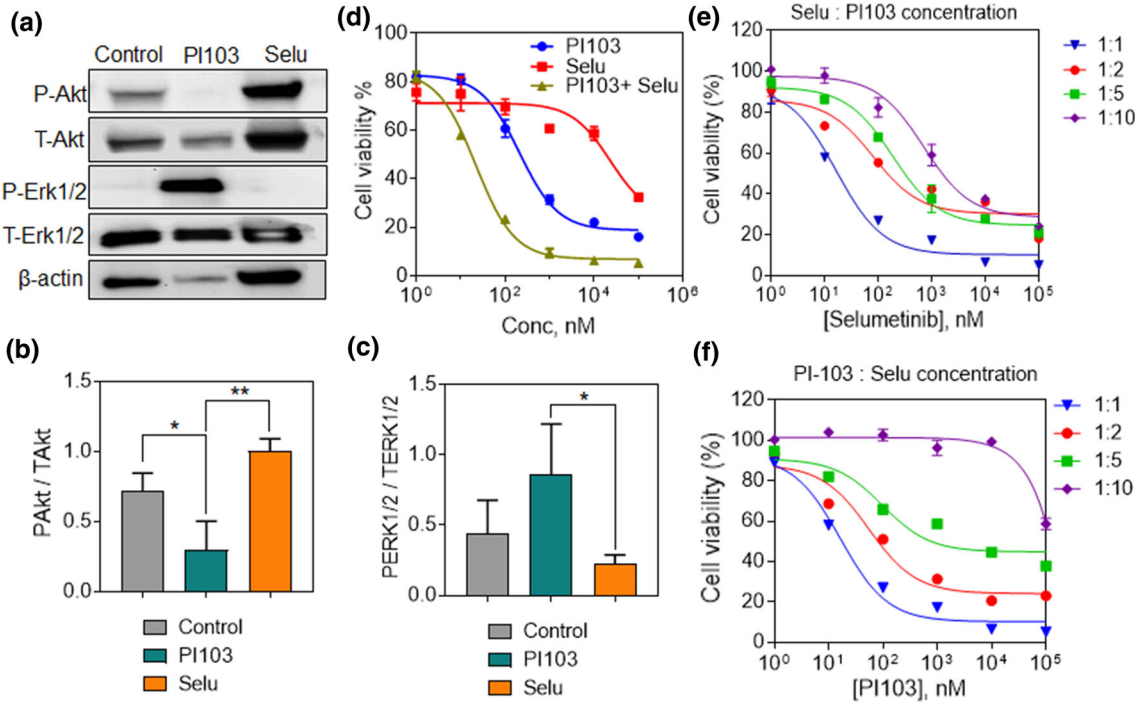

FIGURE 2. Synergistic effect of co-inhibition of PI3K and MAPK pathways in drug-resistance cancer cells: (a) Representative western blot showing differences in expression levels of phospho Erk1/2, Total Erk1/2, phospho Akt and Total Akt in TOV21G ovarian clear cell carcinoma cells after treatments with either 2.5 μM of PI103 or 2.5 μM of Selumetinib. (b-c) Graph showing the quantification of the Erk1/2 and Akt phosphorylation inhibition in TOV21G cells after treatment with either P103 or Selumetinib. Statistical analysis was performed with One-way ANOVA with Newman-Keuls post-test. Data shows mean ± SEM (n = 3); n.s., not significant; *p < 0.05; **p < 0.01; ***p < 0.001. (d) Graph shows effect of increasing concentrations of PI103, Selumetinib and the combination of PI103 and Selumetinib on the viability of TOV21G cells. (e) Graph shows the effect of different ratios of Selumetinib: PI103 ratios on the viability of TOV21G cells. The ratio of Selumetinib was varied while PI103 was kept constant. (f) Graph shows the effect of different ratios of Selumetinib: PI103 ratios on the viability of TOV21G cells. The ratio of PI103 was varied while Selumetinib was kept constant.

based on quantum mechanical all-atomistic simulations.[22,24] Free kinase inhibitors were conjugated to cholesterol hemisuccinate using standard EDC and DMAP reaction. This resulting drug cholesterol conjugates were purified using column chromatography to obtain kinase inhibiting amphiphiles. All-atomistic simulation of a lipid bilayer containing 20 mol% kinase-inhibiting amphiphiles revealed he formation of a stable supramolecular structure (Figs. 3b–3c). In our previous studies, we observed that the kinase inhibiting amphiphiles rapidly self-assemble in the presence of other co-lipids to form stable supramolecular nanoparticles of size around 100 nm.[22,24] This system also allows for higher drug loading as compared to conventional liposomes and drugs concentrations of $>$ 10 mol% could be effectively loaded. Consistent with these observations, we were able to effectively load both kinase inhibiting amphiphiles to form highly stable dual inhibitor-loaded supramolecular nanotherapeutics (DiLNs). 5 mol% MAPK and PI3K-inhibiting amphiphiles (10% total), along with 90% of Co-lipids (60 mol% of PC and 30 mol% of DSPE PEG Amine) self-assembled to form a supramolecular nanotherapeutics (Fig. 3d). Phosphatidylcholine was chosen as a co-lipid for its biocompatibility and a functionalized PEG was used to PEGylate the nanoparticle to increase its circulation half-life. Cryo transmission electron microscopy images revealed that these nanoparticles had a size of around 100 nm and dynamic light scattering (DLS) reveals that the nanoparticles have a hydrodynamic diameter of around 250 nm (Fig. 3e) and the surface zeta potential was found to be 20 mV.

Next, we tested if the DiLNs remained stable for extended periods of time. Size and Zeta potential of the SNPs were measured during storage conditions in PBS at 4 °C. DiLNs showed stable size and zeta potential measurements for over 30 days which proves that these nanoparticles are structurally stable (Figs. 3f–3g). Stability of these SNPs was also measured in biologically relevant conditions such as human serum. Interaction of nanoparticle with biological systems like human blood, causes significant protein adsorption onto the surface of these nanoparticle, hence impacting the size and stability of these particles.[35] DiLNs were incubated in equal volumes of serum, and the size and

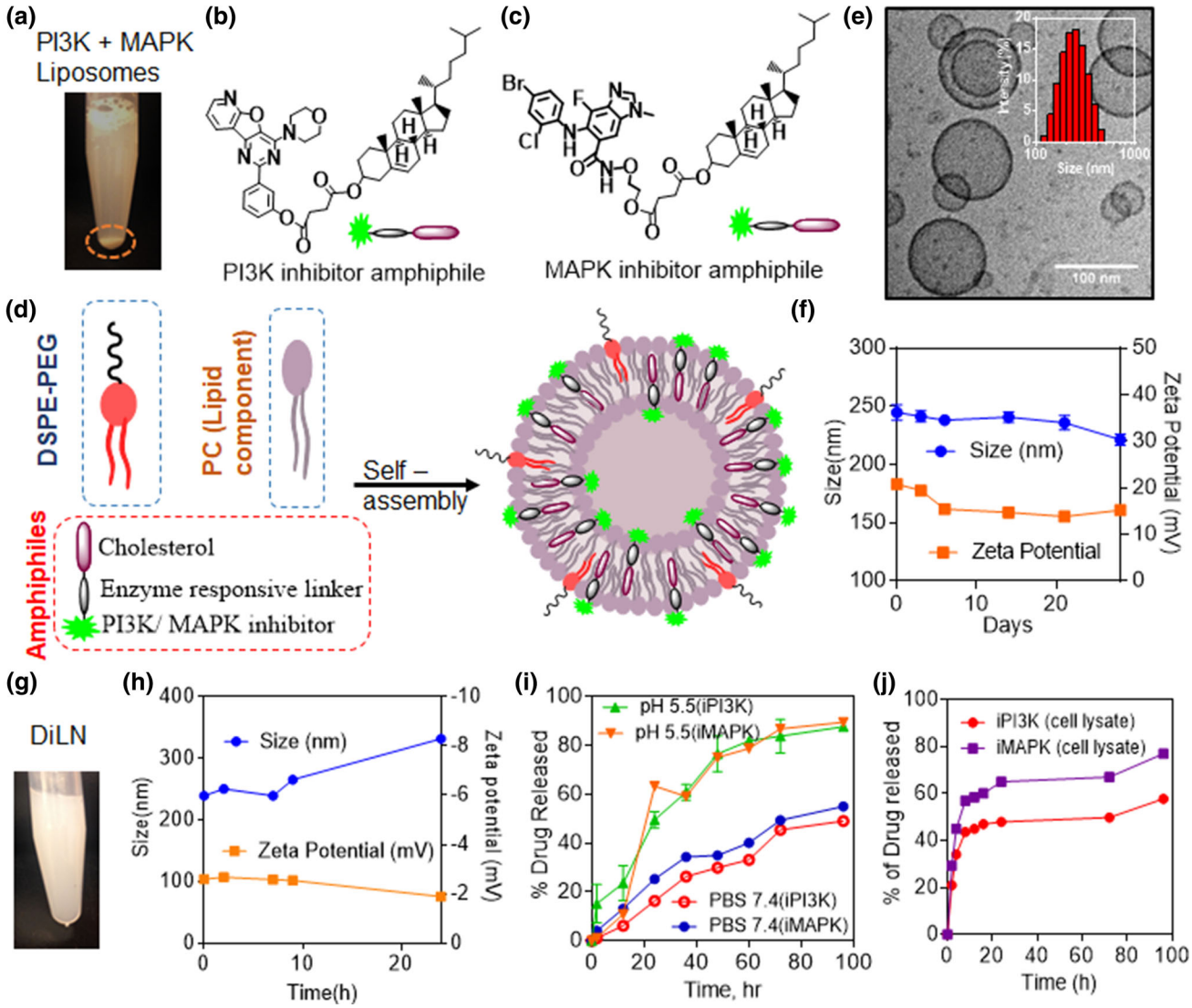

FIGURE 3. DiLNs Synthesis and Characterization: (a) PI103 and Selumetinib loaded liposomes were highly unstable with significant precipitation observed within 10 min of synthesis. (b) Structure of the P13K-inhibiting amphiphile. (c) Structure of the MAPK-inhibiting amphiphile. (d) Schematic representation shows assembly of DiLNs from phosphatidylcholine (PC), P13K inhibitor amphiphile, MAPK inhibitor amphiphile and DSPE-PEG-Amine. (e) High resolution cryo-transmission electron microscopy image (scale bar, 100 nm) of the DiLNs. Insert shows the hydrodynamic size distribution of DiLNs obtained through dynamic light scattering (DLS). (f) Graph shows the physiochemical stability of the DiLNs as a function of the change in size distribution and zeta potential, measured by DLS over a 30-day period. (g) DiLNs maintained the stability for over 30 days with no precipitation observed. (h) Graph shows the stability of the DiLNs when incubated with human serum as a function of the change in size and zeta potential, measured by DLS. (i) Release kinetics profiles of PI3K and MAPK inhibiting amphiphiles at acidic pH (5.5) and physiological pH (7.4). (j) Release kinetics profiles of PI3K and MAPK inhibiting amphiphiles in TOV21G cell lysate.

the zeta potential was measured. DiLNs were shown to be stable for ~ 12 h which validated by the fact that there were minimal changes in the size and zeta potential over the period of that time (Fig. 3h).

After establishing the stability of DiLNs, the drug release profiles were studied at different conditions. The kinase inhibiting amphiphiles have stimuli-responsive linkers which are acid labile. They are pH sensitive and will break down in acidic pH and initiate extended release of the kinase inhibitors. Interestingly, the tumor microenvironment is also acidic and could help in sustained release of the inhibitors from the nanotherapeutics. Moreover, the linkers conjugated to the amphiphiles are also sensitive to the enzyme esterase.[22] Recent studies have highlighted that cancer cells have higher intracellular esterase enzyme levels. [54] We predicted that the action of esterase enzymes on the amphiphiles would further aid in achieving extended drug release profiles. We tested our hypothesis by incubating DiLNs in a buffer which had an acidic pH as well as incubated in PBS to stimulate physiological-relevant pH of 7.4. We observed that there was

a higher incidence of sustained inhibitor release in acidic pH as compared to physiological pH (Fig. 3i). This not only confirmed our hypothesis, but showed that supramolecular constructs can stay in circulation for a longer time without undergoing degradation, releasing the drugs when it reaches the tumor microenvironment. To further validate our results, we also studied the enzymatic and pH mediated extended drug profiles of the kinase inhibiting amphiphiles in TOV21G cell lysate. The cell lysate mimics the activity of enzymes and the pH in the tumor microenvironment. We observed that around 80% of the inhibitors were released from the DiLNs over the period of incubation (Fig. 3j).

In Vitro Efficacy Studies

We next characterized the efficacy of DiLNs in different drug resistant cancer cells. We first wanted to see if DiLNs could effectively internalize into the cells for effective drug delivery. D4M cells were incubated with FITC—tagged DiLNs for different time intervals. After incubation, the cells were then washed, fixed and imaged for fluorescence expression. We observed that DiLNs effectively internalize inside the cell within 4 h with a significant increase in the internalization observed after 12 h (Fig. 4a). Next, we were interested in evaluating the cytotoxic efficacy of DiLNs in TOV21G cells and D4M melanoma cells. We first showed that empty lipid nanoparticles didn't exhibit any toxicity to D4M cancer cells (Suppl. Fig. 3a). Next, equal concentrations of DiLNs, single kinase-inhibitor loaded SNPs and a combination of single kinase inhibitor SNPs were added to the cells. After 72 h of incubation, a cell cytotoxicity assay was performed to evaluate the cytotoxic index of different treatment groups. As shown in the graphs in Figs. 4b–4c and Suppl. Fig. 3c, DiLNs were found to exhibit more cytotoxic efficacy on cancer cells compared to other treatment groups. Interestingly, we also observed that DiLNs performed better than just co-administering equimolar concentrations of single- kinase-inhibiting SNPs. These results are consistent with our previous studies demonstrating that, in models involving synergistic kinase inhibition, delivery of two different drugs in the same nanoparticle proves to more effective than delivery of the individual drugs in two different nanoparticles.[13] Spatial distribution of both the kinase inhibiting amphiphiles into the same cellular compartment ensures that both kinase pathways remains inhibited simultaneously, thus validating our rationale for simultaneous delivery and inhibition of both PI3K and MAPK signaling pathways in the same cell. The fact that both these pathways engage in cross-talk with each other while at the same time compensate for each other's activation further necessitates the need for simultaneous delivery of both kinase-inhibiting amphiphiles in the same delivery system. Next, we performed a western blot analysis to further assess the kinetics of inhibition of MAPK and PI3K pathways by DiLNs as compared to free drugs. We observed that there was similar inhibition of Akt and Erk1/2 at earlier time points but at later time points, sustained kinase inhibition was only shown in groups treated with the DiLNs (Figs. 4d–4f). Recent studies have shown that rebound phosphorylation in kinase pathways happens because of kinase replenishment in the cells due to a positive feedback loop. However, higher internalization of DiLNs in cancer cells coupled with sustained and controlled release of PI3K and MAPK inhibitors results in a sustained inhibition of both the kinase signaling pathways.[23]

T Cell Cytotoxicity and Functionality

The main therapeutic strategy of immune checkpoint inhibition relies on the fact that blocking checkpoints expressed on cancer cells will lead to an increased activation of intratumoral CD8+ T cells, thereby resulting in enhanced anti-tumorigenic efficacy.[29] Recent studies have also highlighted that synergistic effects of combining immunotherapy and targeted therapy resulted in improved T cell activation and tumor infiltration.[34,47,49] The fact that T cell activation and proliferation is controlled by kinase dependent mechanisms, makes it vulnerable to cell death following high dose targeted therapies. However, in contrast, recent studies show that there is a higher incidence of infiltrating cytotoxic CD8+ T cells when treated with PI3K and MAPK inhibitors.[8,49,52] But, as validated by studies done by Denken *et al*., short term targeted treatments are indeed accompanied by high infiltrating intratumoral CD8+ at the start of the treatment but the amount of CD8+ cells significantly decreased at the end stages of the treatment concurrent with the increase in tumor volumes.[8] These observations shows that a major hurdle in effectively enabling a combination of kinase inhibitors with T cell activating immunotherapy is the bioavailability of the kinase inhibitors at the tumor site. Targeted therapies are also dose limited due to high systemic toxicities exhibited on naïve systemic T cells. This entails the need for a delivery system that can deliver kinase inhibitors in a dose dependent manner all the while ensuring sustained release of inhibitors in order to effectively increase intratumoral CD8+ T cells while at the same time reduce systemic T cell death. In order to mimic the effect of DiLNs on systemic naïve T cells, T cells isolated from human PBMCs were treated with increasing concentrations of either the free inhibitor

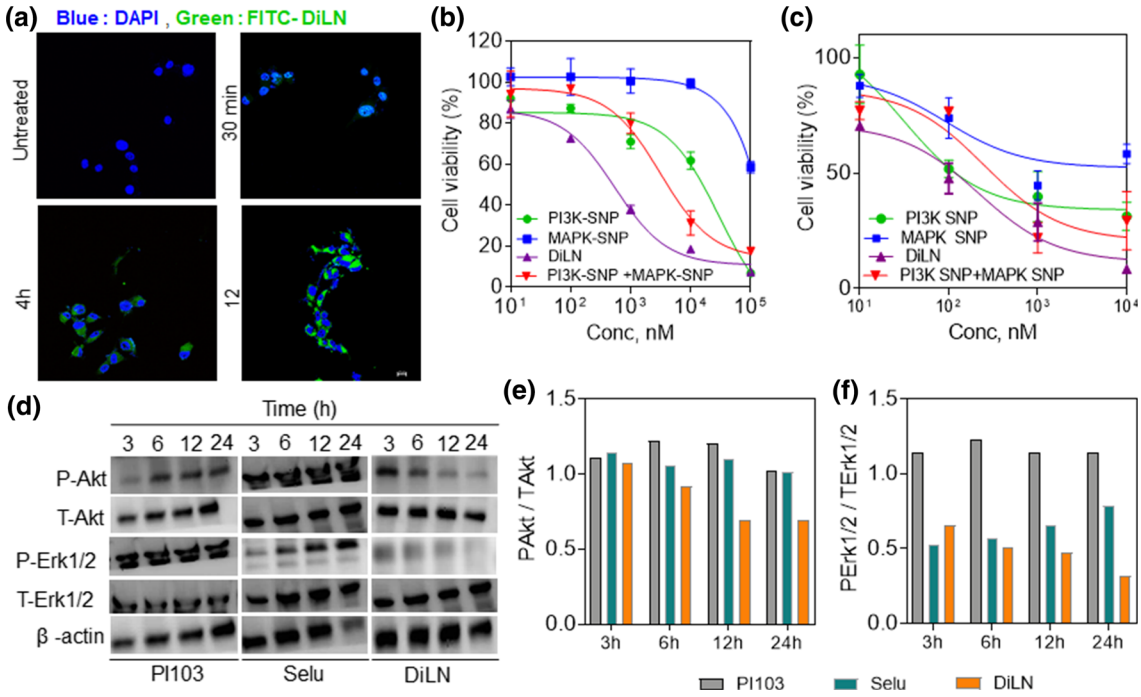

FIGURE 4. ***In vitro*** **efficacy studies: (a) Representative confocal images showing internalization of FITC-tagged DiLNs (green) in D4M cells after 30 min, 4 h and 12 h of nanoparticle incubation. The cells nuclei are stained with DAPI (blue). (b) Graph showing the effect of increasing concentrations of PI3K inhibiting supramolecule (PI3K-SNP), MAPK inhibiting supramolecule (MAPK-SNP), co-administration of PI3K-SNP and MAPK-SNP and DiLNs on the viability of TOV21G Ovarian clear cell carcinoma cells. (c) Graph shows effect of increasing concentrations of PI3K-SNP, MAPK-SNP, co-administration of PI3K-SNP and MAPK-SNP and DiLNs on the viability of D4M cells. (d) Representative western blot showing sustained inhibition of Phospho Akt and Phospho Erk1/2 in TOV21G cells on treatment with either PI103, Selumetinib or DiLNs over time. After 4 h of exposure to drug, the cells were washed thrice with cold PBS to remove additional drug outside cells and then incubated with fresh media with 1% FBS. Cells were collected at 3, 6, 12 and 24 h and probed for protein expression. (e–f) Graph showing the time dependent quantification of the Erk1/2 and Akt phosphorylation inhibition in TOV21G cells after treatment with either P103, Selumetinib or DiLNs.**

combinations or DiLNs. The cytotoxicity index of these drugs on T cells was evaluated by performing a cell cytotoxicity assay and an Annexin V assay. We observed that even at extremely high drug concentrations, DiLNs showed little to no cytotoxicity to T cells, while T cells treated with free drugs were shown to exhibit cell death even at a concentration as low as 100 nM (Fig. 5a). These results were validated using Annexin V/PI staining for apoptosis (Figs. 5c–5d and Suppl. Fig. 3b). This shows that at higher concentrations, sustained drug release by the DiLNs account for lower toxicities since the concentration of the inhibitors don't reach the cytotoxic levels and hence provide a significant advantage over free inhibitors systems. The same principle can also be used to validate the fact that DiLNs did not affect the activation of T cells. T cells obtained from PBMCs were co-incubated with T cell activating CD3/CD28 Dyna beads and increasing concentrations of either DiLNs or combination of free inhibitors. After 36 h of incubation, T cells were stained with a anti CD8+ and anti CD44/anti CD62L antibodies and flow cytometry was performed. We observed that there was no reduction in the number of cytotoxic T cells and effector T cells at the end of the incubation period. We also found an increase in the number of CD8+ T cells (Fig. 5b), in groups treated with DiLNs as compared to free inhibitors which further strengthens that fact that T cells are in fact capable of getting activated in the presence of these kinase inhibitors.

Efficacy Evaluation of Combination of DiLNs with anti PD-L1 Antibody in Immunocompetent D4M Melanoma Model

In order to validate our *in vitro* findings and to study whether the results obtained in terms of sustained parallel inhibition of both MAPK and PI3K pathways using DiLNs can be translated into an animal model, we used a highly aggressive immunocompetent $BRAFV^{600E}$ (D4M) mouse melanoma model to test our hypothesis. We first wanted to quantify the amount of DiLNs that could accumulate into the tumors. D4M tumor bearing mice were injected with NiR dye tagged DiLNs and live mice imaging was done using the *In Vivo* Imaging system (IVIS). The mice were sacrificed after 48 h and their organs were harvested. We observed a time dependent increase in

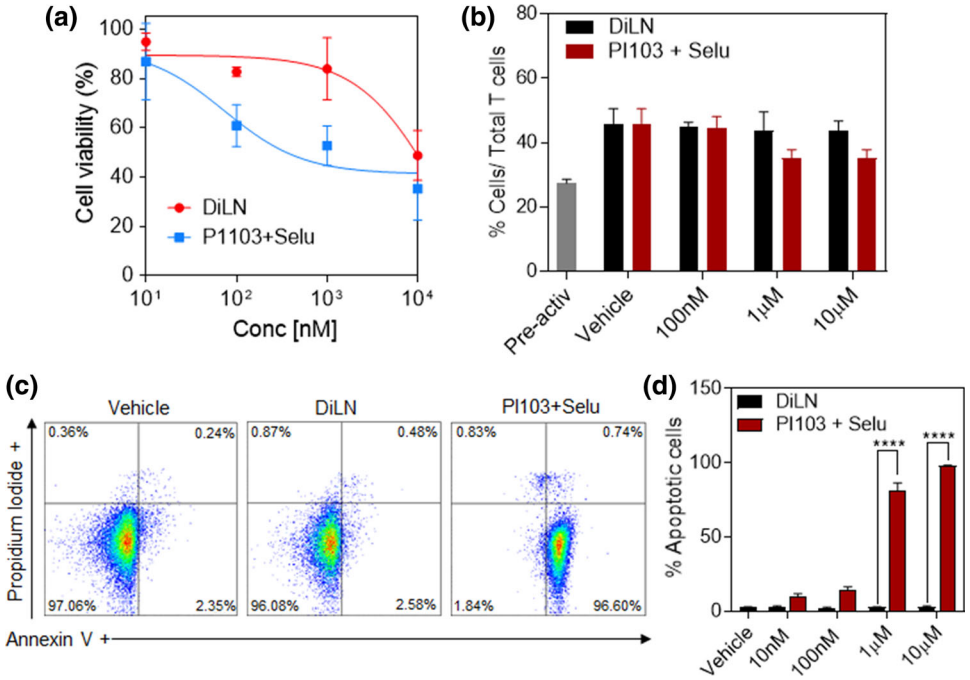

FIGURE 5. T cell cytotoxicity and function: (a) Graph shows the effect of increasing concentrations of combination PI103 and Selumetinib or DiLNs (1:1 drug ratio) on T cells after 72 h of drug treatment. (b) Graph shows the effect of increasing concentrations of PI103 and Selumetinib combined or DiLNs (1:1 drug ratio) on the activity of T cells isolated form PBMCs. T cells were activated using T cell activating CD3/CD28 Dynabeads and co-incubated with either DiLNs or PI103 and Selumetinib. The number of activated T cells (CD8+) was determined by flowcytometry. (c) Representative flow cytometry plots showing apoptosis and necrosis of T cells following treatment with increasing concentration of PI103 + Selumetinib and DiLNs (1:1 drug ratio) as measured by Annexin V Assay. T cells treated with DiLNs induced minimal apoptosis and no significant necrosis. (d) Graph shows the cytotoxic effects of increasing concentrations of either PI103 + Selumetinib or DiLNs (1:1 drug ratio) on T cells. Annexin V was used to determine the number of apoptotic cells. Statistical analysis was performed with student t-test. Data shows mean ± SEM ($n = 3$); ****$p < 0.0001$.

relative fluorescence at the site of the tumor which translated to increased DiLNs accumulation, consistent with our previous findings (Fig. 6a). The harvested tumors and organs were then imaged using the IVIS (Fig. 6b) and the relative fluorescence intensities of the organs were quantified. From the graph shown in (Fig. 6c), we observed that DiLNs accumulate in the tumor at much higher concentration compared to lungs, heart and kidneys. We also observed accumulation of DiLNs in the liver and spleen, which is consistent with RES uptake of DiLNs. Next, we tested if higher accumulation of DiLNs in the tumor could result in higher bioavailability of inhibitors, which in turn could improve anti- tumor efficacy. Mice were subcutaneously injected with D4M cells into the right flanks. When the tumor volume reached 50 mm^3, the mice were randomized into different groups and were subjected to treatments. The treatments consisted of 3 doses of either the DiLNs, DiLNs +Anti PD-L1, Anti PD-L1, PI103 + Selumetinib, PI103 + Selumetinib + Anti PD-L1 or Vehicle. All treatments were normalized to sub-optimal doses of 5 mg/kg of equivalent kinase inhibitor concentration. All doses were administered intravenously except the free drug combinations, which were administered intra peritoneally due to the hydrophobic nature of the drugs. Doses were administered 10 days after the tumor injections. The health of the mice was closely monitored throughout the course of the treatment regimen. Mice were euthanized upon observable necrosis, lethargic movements or if the tumor volume reached 2000 mm^3. Mice from all the groups were euthanized at the same time in order to keep our findings consistent. As shown in Fig. 6d, there was a significant reduction in tumor volume in the group treated with DiLNs as compared to the other groups. Furthermore, survival studies showed that mice treated with DiLNs had increased survival rates as compared to other treatment groups (Fig. 6e).

To understand the mechanisms behind DiLNs efficacy, we performed *ex vivo* analysis of tumor tissues. We wanted to see if combining immune checkpoint inhibition with dual kinase inhibition can result in a synergistic anti-cancer efficacy. We first performed TUNEL staining on tumor sections from different treatments groups and observed significant tumor cell death in the group treated with DiLNs in combination with anti PD-L1 as compared to other groups, these

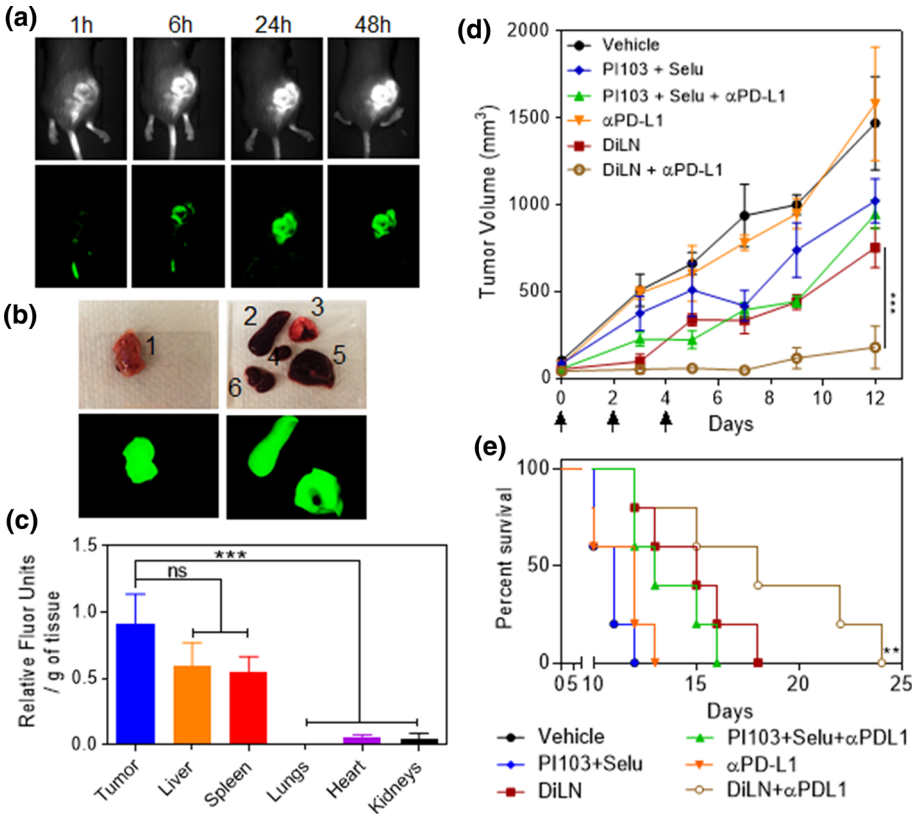

FIGURE 6. Biodistribution study of DiLNs in D4M model: (a) Representative NIR fluorescence images of D4M tumor bearing mice at different time points after NIR-dye tagged DiLNs injection. (b) *Ex-vivo* NIR imaging of the excised organs after 48 h. (1. Tumor, 2. Spleen, 3. Lungs, 4. Heart, 5. Liver 6. Kidneys) (c) Graph shows the quantification of the NIR-dye accumulation in different organs. Data shown are mean ± s. e. m. (n = 3). Statistical analysis was performed with One-way ANOVA with Newman-Keuls post-test. Data shows mean ± SEM (n = 3); n.s., not significant; ***p < 0.001. (d) Graph shows tumor growth profiles in D4M tumor bearing mice after different multi-dose treatments. The tumor bearing animals were injected with 3 doses of either vehicle (control), free drug combination of Selumetinib and PI103, free drug combination of Selumetinib and PI1039 + anti-PD-L1, free anti-PD-L1 antibody, DiLNs and DiLNs + anti-PD-L1 at day 0,3 and 5. (5 mg/kg equivalent dose of each drug-. Data shown are mean ± s. e. m.) (n = 5). Statistical analysis was performed with One-way ANOVA with Newman-Keuls post-test. Data shows mean ± SEM (n = 3); n.s., not significant; ***p < 0.001. (e) Kaplan–Meir survival curves show that treatment with DiLNs increases survival as compared with other treatment groups (n = 5 in each treatment group).

results were consistent with the obtained tumor progression data (Fig. 7a and Suppl. Fig. 4a). Western blot analysis of the tumor lysates revealed a significantly higher inhibition of Phospho-Akt in the groups treated with DiLNs as compared to other groups (Figs. 7b–7d). The higher inhibition of Phospho-Erk1/2 was observed in DiLN + αPD-L1 treated group as compared to DiLN treated group. Flash frozen tumor samples were sectioned and stained with DAPI and FITC anti-CD8a antibody to evaluate the number of infiltrating CD8+ T cells. As expected, we observed a significant infiltration of cytotoxic T cells in the group treated with DiLNs in combination with anti PD-L1 as compare to other treatment groups (Fig. 7e and Suppl Fig. 4b). This further proves our hypothesis that sustained release of dual inhibiting kinases synergizes with T cell activation pathways which results in a higher incidence of infiltrating cytotoxic T cells in the tumor and enhanced anti-cancer efficacy.

CONCLUSION

In conclusion, we have synthesized a self-assembled lipid-based DiLNs which can be simultaneously loaded with two kinase inhibitors targeting the PI3K and MAPK signaling pathways. These DiLNs were stable and could simultaneously deliver active inhibitors at very high concentrations by preferentially homing into the tumor and releasing its payload. Sustained release of these inhibitors in a dose dependent manner resulted in a sustained inhibition of kinase signaling pathways while significantly reducing systemic T cell toxicity. In addition to this, rational combination of DiLNs with a PD-L1 immune checkpoint inhibitor significantly improved anti-cancer efficacy due to synergistic effects of kinase inhibition and enhanced immune response facilitated by increased T cell activation as observed by higher intratumoral CD8+ effector T cells. This novel

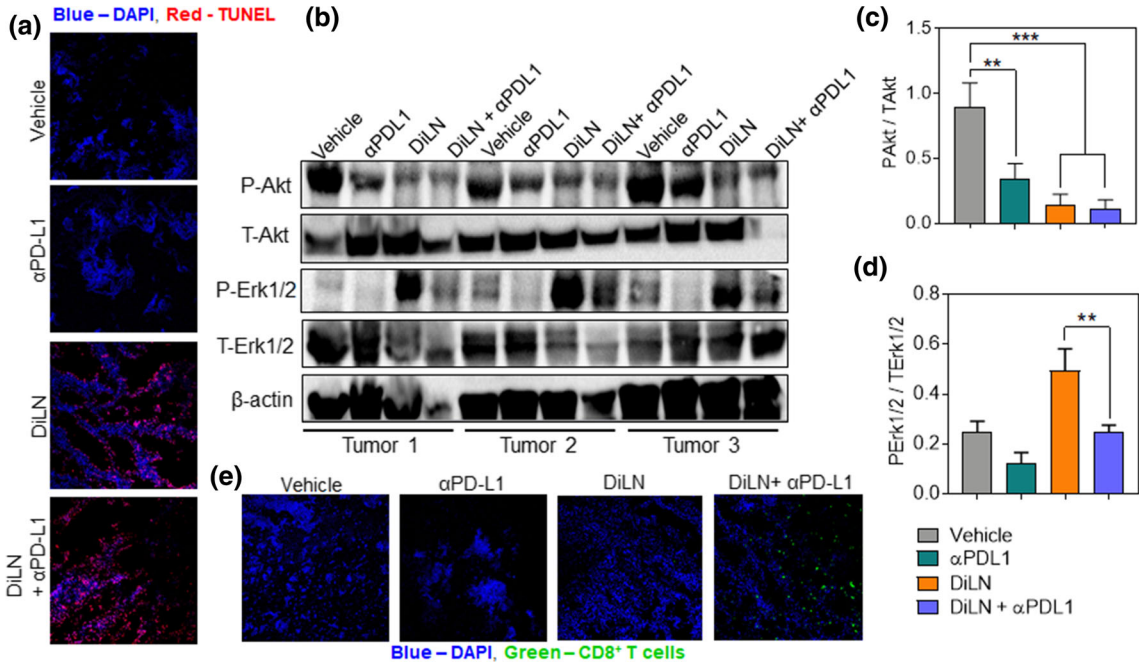

FIGURE 7. ***Ex vivo*** **studies: (a) The tumors were excised post-treatment and processed for terminal deoxynucleotidyl transferase dUTP nick end labeling (TUNEL) as a marker for apoptosis. Treatment with DiLNs resulted in more apoptosis as compared to the other treatment groups. (b) Western blot showing expression of Phospho Erk1/2, Total Erk1/2, Phospho Akt, Total Akt in tumors lysates taken from different treatment groups. *β*-actin was used for normalization (c-d) Graph showing the quantification of the Erk1/2 and Akt phosphorylation inhibition in tumors lysates taken from different treatment groups. Statistical analysis was performed with One-way ANOVA with Newman-Keuls post-test. Data shows mean ± SEM ($n = 3$); $^{**}p < 0.01$; $^{***}p < 0.001$ (e) Representative fluorescence images show CD8+ (Green) T cells in cross-sections of tumor tissue from different treatment groups.**

method could pave the way in enabling rational strategies for combining targeted therapies with immunotherapy approaches thereby improving anti-cancer efficacy in aggressive chemotherapy-resistant models.

ELECTRONIC SUPPLEMENTARY MATERIAL

The online version of this article (https://doi.org/10.1007/s12195-019-00576-1) contains supplementary material, which is available to authorized users.

ACKNOWLEDGMENTS

We are extremely grateful for the support offered by the Brigham & Women's Hospital Young Investigator Award, Melanoma Research Alliance Young Investigator Award (510283) and Cancer Research Institute (118-1501) Technology Impact Award to A. K. We would like to thank the BWH animal facility for their help with *in vivo* imaging. We thank the Biophysical Characterization Core at the Institute for Applied Life Sciences (IALS), University of Massachusetts Amherst for lending their expertise in regards to characterization experiments. We would also like thank Light Microscopy Core facility at University of Massachusetts Amherst for their help and consultation while performing confocal imaging.

CONFLICT OF INTEREST

Anujan Ramesh, Siva Kumar Natarajan, Dipika Nandi and Ashish Kulkarni declare that they have no conflicts of interest.

RESEARCH INVOLVING IN HUMAN AND ANIMAL STUDIES

All institutional and national guidelines for the care and use of laboratory animals were followed and approved by the appropriate institutional committees. No human studies were carried out by the authors for this article.

REFERENCES

[1]Bekaii-Saab, T., *et al*. Multi-institutional phase II study of selumetinib in patients with metastatic biliary cancers. *J. Clin. Oncol.* 29:2357–2363, 2011. https://doi.org/10.1200/JCO.2010.33.9473.

[2]Brahmer, J. R., *et al*. Safety and activity of anti-PD-L1 antibody in patients with advanced cancer. *N. Engl. J. Med.* 366:2455–2465, 2012. https://doi.org/10.1056/NEJMoa1200694.
[3]Burotto, M., V. L. Chiou, J. M. Lee, and E. C. Kohn. The MAPK pathway across different malignancies: a new perspective. *Cancer* 120:3446–3456, 2014. https://doi.org/10.1002/cncr.28864.
[4]Cho, K., X. Wang, S. Nie, Z. G. Chen, and D. M. Shin. Therapeutic nanoparticles for drug delivery in cancer. *Clin. Cancer Res* 14:1310–1316, 2008. https://doi.org/10.1158/1078-0432.CCR-07-1441.
[5]Choi, K. C., N. Auersperg, and P. C. Leung. Mitogen-activated protein kinases in normal and (pre)neoplastic ovarian surface epithelium. *Reprod Biol Endocrinol* 1:71, 2003. https://doi.org/10.1186/1477-7827-1-71.
[6]Coates, A., *et al*. On the receiving end–patient perception of the side-effects of cancer chemotherapy. *Eur. J. Cancer Clin. Oncol.* 19:203–208, 1983.
[7]Davis, M. E., Z. G. Chen, and D. M. Shin. Nanoparticle therapeutics: an emerging treatment modality for cancer. *Nat. Rev. Drug Discov.* 7:771–782, 2008. https://doi.org/10.1038/nrd2614.
[8]Deken, M. A., *et al*. Targeting the MAPK and PI3K pathways in combination with PD1 blockade in melanoma. *Oncoimmunology* 5:e1238557, 2016. https://doi.org/10.1080/2162402X.2016.1238557.
[9]Dhillon, A. S., S. Hagan, O. Rath, and W. Kolch. MAP kinase signalling pathways in cancer. *Oncogene* 26:3279, 2007. https://doi.org/10.1038/sj.onc.1210421.
[10]Dienstmann, R., J. Rodon, V. Serra, and J. Tabernero. Picking the point of inhibition: a comparative review of PI3K/AKT/mTOR pathway inhibitors. *Mol Cancer Ther.* 13:1021–1031, 2014. https://doi.org/10.1158/1535-7163.MCT-13-0639.
[11]Eliopoulos, A. G., *et al*. The control of apoptosis and drug resistance in ovarian cancer: influence of p53 and Bcl-2. *Oncogene* 11:1217–1228, 1995.
[12]Fruman, D. A., *et al*. The PI3K pathway in human disease. *Cell* 170:605–635, 2017. https://doi.org/10.1016/j.cell.2017.07.029.
[13]Goldman, A., *et al*. Rationally designed 2-in-1 nanoparticles can overcome adaptive resistance in cancer. *ACS Nano* 10:5823–5834, 2016. https://doi.org/10.1021/acsnano.6b00320.
[14]Holderfield, M., M. M. Deuker, F. McCormick, and M. McMahon. Targeting RAF kinases for cancer therapy: BRAF-mutated melanoma and beyond. *Nat. Rev. Cancer* 14:455–467, 2014. https://doi.org/10.1038/nrc3760.
[15]Holohan, C., S. Van Schaeybroeck, D. B. Longley, and P. G. Johnston. Cancer drug resistance: an evolving paradigm. *Nat. Rev. Cancer* 13:714–726, 2013. https://doi.org/10.1038/nrc3599.
[16]Hong, D. S., *et al*. A multicenter phase I trial of PX-866, an oral irreversible phosphatidylinositol 3-kinase inhibitor, in patients with advanced solid tumors. *Clin. Cancer Res.* 18:4173–4182, 2012. https://doi.org/10.1158/1078-0432.CCR-12-0714.
[17]Housman, G., *et al*. Drug resistance in cancer: an overview. *Cancers (Basel)* 6:1769–1792, 2014. https://doi.org/10.3390/cancers6031769.
[18]Inamdar, G. S., S. V. Madhunapantula, and G. P. Robertson. Targeting the MAPK pathway in melanoma: why some approaches succeed and other fail. *Biochem. Pharmacol.* 80:624–637, 2010. https://doi.org/10.1016/j.bcp.2010.04.029.
[19]Janku, F., T. A. Yap, and F. Meric-Bernstam. Targeting the PI3K pathway in cancer: are we making headway? *Nat. Rev. Clin. Oncol.* 15:273–291, 2018. https://doi.org/10.1038/nrclinonc.2018.28.
[20]Kim, E. H., and M. Suresh. Role of PI3K/Akt signaling in memory CD8 T cell differentiation. *Front. Immunol.* 4:20, 2013. https://doi.org/10.3389/fimmu.2013.00020.
[21]Kirkwood, J. M., *et al*. Next generation of immunotherapy for melanoma. *J. Clin. Oncol.* 26:3445–3455, 2008. https://doi.org/10.1200/JCO.2007.14.6423.
[22]Kulkarni, A., S. K. Natarajan, V. Chandrasekar, P. R. Pandey, and S. Sengupta. Combining immune checkpoint inhibitors and kinase-inhibiting supramolecular therapeutics for enhanced anticancer efficacy. *ACS Nano* 10:9227–9242, 2016. https://doi.org/10.1021/acsnano.6b01600.
[23]Kulkarni, A. A., *et al*. Supramolecular nanoparticles that target phosphoinositide-3-kinase overcome insulin resistance and exert pronounced antitumor efficacy. *Cancer Res* 73:6987–6997, 2013. https://doi.org/10.1158/0008-5472.CAN-12-4477.
[24]Kulkarni, A., *et al*. A designer self-assembled supramolecule amplifies macrophage immune responses against aggressive cancer. *Nat. Biomed. Eng.* 2:589–599, 2018. https://doi.org/10.1038/s41551-018-0254-6.
[25]Kwong, L. N., and M. A. Davies. Navigating the therapeutic complexity of PI3K pathway inhibition in melanoma. *Clin. Cancer Res.* 19:5310–5319, 2013. https://doi.org/10.1158/1078-0432.CCR-13-0142.
[26]Lee, S., E. J. Choi, C. Jin, and D. H. Kim. Activation of PI3K/Akt pathway by PTEN reduction and PIK3CA mRNA amplification contributes to cisplatin resistance in an ovarian cancer cell line. *Gynecol Oncol* 97:26–34, 2005. https://doi.org/10.1016/j.ygyno.2004.11.051.
[27]Long, G. V., *et al*. Combined BRAF and MEK inhibition versus BRAF inhibition alone in melanoma. *N. Engl. J. Med.* 371:1877–1888, 2014. https://doi.org/10.1056/NEJMoa1406037.
[28]Mabuchi, S., T. Sugiyama, and T. Kimura. Clear cell carcinoma of the ovary: molecular insights and future therapeutic perspectives. *J. Gynecol. Oncol.* 27:e31, 2016. https://doi.org/10.3802/jgo.2016.27.e31.
[29]Mahoney, K. M., G. J. Freeman, and D. F. McDermott. The next immune-checkpoint inhibitors: PD-1/PD-L1 blockade in melanoma. *Clin Ther* 37:764–782, 2015. https://doi.org/10.1016/j.clinthera.2015.02.018.
[30]Manzano, J. L., *et al*. Resistant mechanisms to BRAF inhibitors in melanoma. *Ann. Transl. Med.* 4:237, 2016. https://doi.org/10.21037/atm.2016.06.07.
[31]Mayer, I. A., and C. L. Arteaga. The PI3K/AKT pathway as a target for cancer treatment. *Annu Rev. Med.* 67:11–28, 2016. https://doi.org/10.1146/annurev-med-062913-051343.
[32]Mendoza, M. C., E. E. Er, and J. Blenis. The Ras-ERK and PI3K-mTOR pathways: cross-talk and compensation. *Trends Biochem. Sci.* 36:320–328, 2011. https://doi.org/10.1016/j.tibs.2011.03.006.
[33]Park, S., *et al*. PI-103, a dual inhibitor of Class IA phosphatidylinositide 3-kinase and mTOR, has antileukemic activity in AML. *Leukemia* 22:1698–1706, 2008. https://doi.org/10.1038/leu.2008.144.
[34]Peng, W., *et al*. Loss of PTEN promotes resistance to T cell-mediated immunotherapy. *Cancer Discov* 6:202–216, 2016. https://doi.org/10.1158/2159-8290.CD-15-0283.

[35]Pino, P. D., *et al*. Protein corona formation around nanoparticles—from the past to the future. *Mater. Horiz.* 1:301–313, 2014. https://doi.org/10.1039/c3mh00106g.
[36]Pons-Tostivint, E., B. Thibault, and J. Guillermet-Guibert. Targeting PI3K signaling in combination cancer therapy. *Trends Cancer* 3:454–469, 2017. https://doi.org/10.1016/j.trecan.2017.04.002.
[37]Prieto, P. A., *et al*. CTLA-4 blockade with ipilimumab: long-term follow-up of 177 patients with metastatic melanoma. *Clin. Cancer Res.* 18:2039–2047, 2012. https://doi.org/10.1158/1078-0432.CCR-11-1823.
[38]Raynaud, F. I., *et al*. Biological properties of potent inhibitors of class I phosphatidylinositide 3-kinases: from PI-103 through PI-540, PI-620 to the oral agent GDC-0941. *Mol. Cancer Ther.* 8:1725–1738, 2009. https://doi.org/10.1158/1535-7163.MCT-08-1200.
[39]Santarpia, L., S. M. Lippman, and A. K. El-Naggar. Targeting the MAPK-RAS-RAF signaling pathway in cancer therapy. *Expert Opin. Ther. Targets* 16:103–119, 2012. https://doi.org/10.1517/14728222.2011.645805.
[40]Sarker, D., *et al*. First-in-human phase I study of pictilisib (GDC-0941), a potent pan-class I phosphatidylinositol-3-kinase (PI3K) inhibitor, in patients with advanced solid tumors. *Clin. Cancer Res.* 21:77–86, 2015. https://doi.org/10.1158/1078-0432.CCR-14-0947.
[41]Shapiro, G. I., *et al*. Phase I safety, pharmacokinetic, and pharmacodynamic study of SAR245408 (XL147), an oral pan-class I PI3K inhibitor, in patients with advanced solid tumors. *Clin. Cancer Res.* 20:233–245, 2014. https://doi.org/10.1158/1078-0432.CCR-13-1777.
[42]Sharp, L. L., D. A. Schwarz, C. M. Bott, C. J. Marshall, and S. M. Hedrick. The influence of the MAPK pathway on T cell lineage commitment. *Immunity* 7:609–618, 1997.
[43]Siegel, R. L., K. D. Miller, and A. Jemal. Cancer statistics, 2018. *CA Cancer. J. Clin.* 68:7–30, 2018. https://doi.org/10.3322/caac.21442.
[44]Smalley, K. S., *et al*. Multiple signaling pathways must be targeted to overcome drug resistance in cell lines derived from melanoma metastases. *Mol Cancer Ther* 5:1136–1144, 2006. https://doi.org/10.1158/1535-7163.MCT-06-0084.
[45]Sordella, R., D. W. Bell, D. A. Haber, and J. Settleman. Gefitinib-sensitizing EGFR mutations in lung cancer activate anti-apoptotic pathways. *Science* 305:1163–1167, 2004. https://doi.org/10.1126/science.1101637.
[46]Topalian, S. L., C. G. Drake, and D. M. Pardoll. Immune checkpoint blockade: a common denominator approach to cancer therapy. *Cancer Cell* 27:450–461, 2015. https://doi.org/10.1016/j.ccell.2015.03.001.
[47]Vanneman, M., and G. Dranoff. Combining immunotherapy and targeted therapies in cancer treatment. *Nat Rev. Cancer* 12:237–251, 2012. https://doi.org/10.1038/nrc3237.
[48]Vara, J. A. F., *et al*. PI3K/Akt signalling pathway and cancer. *Cancer Treat Rev* 30:193–204, 2004. https://doi.org/10.1016/j.ctrv.2003.07.007.
[49]Vella, L. J., *et al*. MEK inhibition, alone or in combination with BRAF inhibition, affects multiple functions of isolated normal human lymphocytes and dendritic cells. *Cancer Immunol Res* 2:351–360, 2014. https://doi.org/10.1158/2326-6066.CIR-13-0181.
[50]Villanueva, J., *et al*. Acquired resistance to BRAF inhibitors mediated by a RAF kinase switch in melanoma can be overcome by cotargeting MEK and IGF-1R/PI3K. *Cancer Cell* 18:683–695, 2010. https://doi.org/10.1016/j.ccr.2010.11.023.
[51]Wang, X., *et al*. Tumor suppressor miR-34a targets PD-L1 and functions as a potential immunotherapeutic target in acute myeloid leukemia. *Cell. Signal.* 27:443–452, 2015. https://doi.org/10.1016/j.cellsig.2014.12.003.
[52]Wilmott, J. S., *et al*. Selective BRAF inhibitors induce marked T-cell infiltration into human metastatic melanoma. *Clin. Cancer Res.* 18:1386–1394, 2012. https://doi.org/10.1158/1078-0432.CCR-11-2479.
[53]Xu, S., *et al*. miR-424(322) reverses chemoresistance via T-cell immune response activation by blocking the PD-L1 immune checkpoint. *Nat Commun* 7:11406, 2016. https://doi.org/10.1038/ncomms11406.
[54]Yamazaki, Y., *et al*. Difference between cancer cells and the corresponding normal tissue in view of stereoselective hydrolysis of synthetic esters. *Biochim. Biophys. Acta* 1243:300–308, 1995.
[55]Zhao, Y., and A. A. Adjei. The clinical development of MEK inhibitors. *Nat. Rev. Clin. Oncol.* 11:385–400, 2014. https://doi.org/10.1038/nrclinonc.2014.83.

Publisher's Note Springer Nature remains neutral with regard to jurisdictional claims in published maps and institutional affiliations.